Virginia Commonwealth University
VCU Scholars Compass

Electrical and Computer Engineering Publications

Dept. of Electrical and Computer Engineering

2005

Dielectric functions and electronic band structure of lead zirconate titanate thin films

Hosun Lee
Virginia Commonwealth University

Youn Seon Kang
Virginia Commonwealth University

Sang-Jun Cho
Virginia Commonwealth University

See next page for additional authors

Authors

Hosun Lee, Youn Seon Kang, Sang-Jun Cho, Bo Xiao, Hadis Morkoç, Tae Dong Kang, Ghil Soo Lee, Jingbo Li, Su-Huai Wei, P. G. Snyder, and J. T. Evans

Dielectric functions and electronic band structure of lead zirconate titanate thin films

Hosun Lee,[a] Youn Seon Kang, Sang-Jun Cho, Bo Xiao, and Hadis Morkoç
Department of Electrical Engineering, Virginia Commonwealth University, 601 W. Main Street, Richmond, Virginia 23284

Tae Dong Kang and Ghil Soo Lee
Department of Physics, Kyung Hee University, Suwon 449-701, South Korea

Jingbo Li and Su-Huai Wei
National Renewable Energy Laboratory, Golden, Colorado 80401

P. G. Snyder
Department of Electrical Engineering, University of Nebraska-Lincoln, Lincoln, Nebraska 68588

J. T. Evans
Radiant Technology Inc., 2021 Girard Blvd, SE3. Albuquerque, New Mexico 87106

We measure pseudodielectric functions in the visible-deep ultraviolet spectral range of $Pb(Zr_xTi_{1-x})O_3$ ($x = 0.2, 0.56, 0.82$) (PZT), $Pb_{0.98}Nb_{0.04}(Zr_{0.2}Ti_{0.8})_{0.96}O_3$, $Pb_{0.91}La_{0.09}(Zr_{0.65}Ti_{0.35})_{0.98}O_3$, and $Pb_{0.85}La_{0.15}Ti_{0.96}O_3$ films grown on platinized silicon substrates using a sol-gel method and on (0001) sapphire using a radio-frequency sputtering method. Using a parametric optical constant model, we estimate the dielectric functions (ϵ) of the perovskite oxide thin films. Taking the second derivative of the fitted layer dielectric functions and using the standard critical-point model, we determine the parameters of the critical points. In the second derivative spectra, the lowest band-gap energy peak near 4 eV is fitted as a double peak for annealed PZTs due to the perovskite phase. As-grown PZTs have mainly pyrochlore phase and the lowest band-gap peak is fitted as a single peak. We also examine the effect of dopants La and Nb, which substitute at Pb and Zr (Ti) sites, respectively. We found three band gaps E_a ($\sim$3.9 eV), E_b ($\sim$4.5 eV), and E_c ($\sim$6.5 eV) in the order of increasing energy. The E_a and E_b band-gap energies were not sensitive to Zr composition. We discuss the change of critical-point parameters for PZTs in comparison to the band-structure calculations based on local-density approximation. The near constancy of the lowest band-gap energy independent of Zr composition is consistent with the band-structure calculations. © *2005 American Institute of Physics.* [DOI: 10.1063/1.2128043]

I. INTRODUCTION

Perovskite oxide materials have very wide applications: various sensors, nonvolatile and dynamic random access memories, tunable capacitors for high-frequency microwave applications, electro-optic modulators, infrared detectors, and microelectromechanical systems.[1,2] Hybridized semiconductors including perovskite oxide materials are being investigated intensively.[3] Among various perovskite oxide materials, $Pb(Zr_xTi_{1-x})O_3$ (PZT) is the most widely commercialized due to its excellent ferroelectric and piezoelectric material properties notwithstanding fatigue.[4] The interface degradation between PZT layer and metal electrodes is known to be the main cause for fatigue of PZT.[5] Other lead-free perovskite oxide materials such as $Ba_{1-x}Sr_xTiO_3$, $SrBi_2Ta_2O_9$, and $Bi_{3.25}La_{0.75}Ti_3O_{12}$ are being investigated as alternatives because of health and environmental concerns as well as fatigue-free properties.

Electrical properties of PZTs have been investigated intensively.[5] However, optical properties of PZT are relatively less investigated.[6,7] Spectroscopic ellipsometry can measure dielectric functions (ϵ) of ferroelectric thin films and subsequently can provide electronic band-structure information as well as thickness and microstructure. Several ellipsometric investigations have been reported.[7,8] However, their spectral range was limited to the region below and near the lowest band-gap region, that is, between 1.5 and 5 eV.[7,8] Ellipsometric studies have not been done which cover the near-infrared (NIR) to deep ultraviolet (DUV) spectral region.

PZT-based devices show excellent ferroelectric properties such as high remanent polarization and low coercive electric field. Semiconducting properties of PZT perovskite oxides have also been reported by using current-voltage measurements by Pintile *et al.*[9] and Boerasu *et al.*[10] They noted that a large concentration of defects can act as trapping centers and that Schottky barriers can be present at contacts instead.

In order to obtain superior ferroelectric and piezoelectric properties, perovskite oxides (ABO_3) must be annealed after deposition to increase the perovskite phase. However, the

[a] Permanent address: Department of Physics, Kyung Hee University, Suwon 449-701, South Korea, on sabbatical leave; electronic mail: hlee@khu.ac.kr

perovskite phase may not result because of the incomplete transformation from pyrochlore phase ($A_2B_2O_7$), which lacks ferro- and piezoelectric properties.[11]

The properties of PZT films can be modified optically and electrically by the addition of foreign ions, for example, La and Nb, substituting for host atoms [Pb, Zr (Ti)]. The addition of donor dopants reduces the concentration of intrinsic oxygen vacancies caused by PbO evaporation during the growth and annealing of PZT thin films. Electrons from donors compensate holes from acceptor impurities originating from Pb vacancies. The transparent $Pb_{1-x}La_x(Zr_yTi_{1-y})_{1-0.25x}O_3$ (PLZT) films have distinguished electro-optic effects and excellent relaxor properties, and have improved various material characteristics: dielectric, ferroelectric, piezoelectric, electro-optic, and pyroelectric behaviors.[12] In general, relaxor behavior is characterized by a broad maximum in the temperature dependence of dielectric property, and a strong frequency dispersion of the permittivity at temperatures around and below the transition temperature. Nb dopant increases the electrical resistance of $Pb_{1-0.5x}Nb_x(Zr_yTi_{1-y})_{1-x}O_3$ (PNZT) thin films and produces polarization hysterisis loops with low coercive fields and large remanent polarizations.[13] $Pb_{1-x}La_xTi_{1-x/4}O_3$ (PLT) also has interesting properties of dielectric, ferroelectric, pyroelectric, piezoelectric, and nonlinear electro-optic properties. Particularly, relaxor behavior is observed.[14]

In this work, we measured the pseudodielectric functions of PZTs, PLT, and doped PZTs. Using a parametric optical constant (POC) model, we estimated the dielectric functions of PZT layers and determined the critical-point (CP) parameters by performing a standard critical-point (SCP) model analysis. The determined band-gap values are consistent with literature values. The lowest band gaps are fitted as a double peak (E_a and E_b), and the band-gap energies are almost constant, independent of Zr composition. We also compared the experimentally determined band-gap values with those of band-structure calculations of local-density approximation (LDA). The calculated results showed that PZT has a direct band gap at the X point and that the band-gap energy is almost constant as a function of Zr composition.

II. EXPERIMENTS

We grew $Pb(Zr_xTi_{1-x})O_3$ ($x=0.56$ and 0.82) (abbreviated as PZT56 and PZT82) samples on sapphire (Al_2O_3) using rf magnetron sputtering methods. We also grew $Pb(Zr_{0.2}Ti_{0.8})O_3$ (abbreviated as PZT20), $Pb_{0.98}Nb_{0.04}(Zr_{0.2}Ti_{0.8})_{0.96}O_3$ (abbreviated as PNZT), $Pb_{0.91}La_{0.09}(Zr_{0.65}Ti_{0.35})_{0.98}O_3$ (abbreviated as PLZT), and $Pb_{0.85}La_{0.15}Ti_{0.96}O_3$ (abbreviated as PLT) thin films using sol-gel methods on platinized silicon ($Pt/TiO_2/SiO_2/Si$) at Radiant Technologies.

We used rf sputtering to grow PZT56 and PZT82 on sapphire. The growth temperature was measured to be 410 °C, and rf power was 200 W. The argon and oxygen gas flow rates were 40 and 19 SCCM (standard cubic centimeter per minute), respectively. We used a nominal $Pb_{1.2}(Zr_{0.5}Ti_{0.5})O_3$ target of 20% excess Pb, adopted a rotat-

ing substrate holder, and used additional Zr and Ti pellets to control stoichiometry. The PZT samples were annealed at 800 °C in air to obtain the perovskite phase.

PZT, PLT, PNZT, and PLZT thin films with 270 nm thickness were grown using sol-gel process on platinized silicon wafer. The structure of the platinized silicon was $Pt(150 \text{ nm})/TiO_2(40 \text{ nm})/SiO_2(500 \text{ nm})/(100)$ silicon substrate. The Pt and TiO_2 layers were deposited by *e*-beam deposition. PZT layers were crystallized by annealing in oxygen ambient at a temperature of 650 °C. Ferroelectric capacitors were fabricated from PZT, PLT, PNZT, and PLZT samples and tested using ferroelectric testers at Radiant Technologies. They showed excellent ferroelectric hysteresis behavior in terms of low coercive bias voltage and large remanent polarization. For example, the PNZT layer had a coercive bias voltage of 2 V and remanent polarization of 18 $\mu C/cm^2$.

Microstructure and crystal orientation were determined using a conventional x-ray diffractometer (MacScience Model M18XHF, maximum power 18 kW). The compositions were determined by using energy-dispersive x-ray spectrometry (EDS). We estimated surface roughness with atomic force microscopy (AutoProbe CP Research System, Thermo Microscope Inc.). Surface morphology of the samples was diagnosed with scanning electron microscopy. The x-ray and atomic force microscopy (AFM) results are summarized in Table I.

Spectroscopic ellipsometric measurements were performed using variable angle spectroscopic ellipsometry and vacuum ultraviolet spectroscopic ellipsometry (J. A. Woollam Co.) at incidence angles of 60°, 65°, 70°, and 75° using an autoretarder. Multiangle capability increases the accuracy of layer modeling.

III. RESULTS

A. X ray and microstructure

Figures 1(a)–1(h) show the x-ray data of the PZT, PLT, and doped PZT thin films. PZT56 and PZT82 which were sputter grown on sapphire and annealed showed higher crystallinity than PZT20, PLT, PNZT, and PLZT samples sol-gel grown on platinized silicon substrates because the x-ray intensity from the perovskite phase was much higher for the sputter-grown and annealed samples. As-grown PZTs using sputter deposition have mainly the pyrochlore phase with a small proportion of the perovskite phase as shown in Figs. 1(a) and 1(c).[15] Table I lists the main x-ray peaks from the perovskite phase of annealed PZTs and those of the pyrochlore phase from as-grown PZTs. PZTs grown on platinized silicon wafer using the sol-gel method have mainly (001) perovskite phase, whereas PZTs grown using the sputtering method have mainly the (111) phase for PZT56 and mainly the (110) phase for PZT82. Sample microstructure and crystal orientation can be affected by Zr composition, buffer and substrate effects, annealing condition, and growth methods. A morphotropic phase boundary of tetragonal to rhombohedral phase transition occurs at Zr=0.53 for bulk PZT

TABLE I. Thickness and volume fraction of void in surface roughness layer. The thickness of the main layer was determined by ellipsometry. AFM-measured roughness and the main x-ray peaks are listed with crystal phase (Pv: perovskite, Pr: pyrochlore), substrate, and growth method.

	Main layer thickness (nm)	Roughness layer thickness (nm), void fraction (%)	AFM rms roughness (nm)	Main x-ray peak	Substrate, growth method
$Pb(Zr_{0.2}Ti_{0.8})O_3$	204.0	9.1, 29.8	2.05	Pv (100)	Platinized Si, sol gel
$Pb(Zr_{0.56}Ti_{0.44})O_3$, as grown	367.9	6.2, 22.1		Pr (400)	Al_2O_3, sputter
$Pb(Zr_{0.56}Ti_{0.44})O_3$	339.9	16.7, 28.8	5.27	Pv(111)	Al_2O_3, sputter
$Pb(Zr_{0.82}Ti_{0.18})O_3$, as grown	188.8	9.9, 19.5		Pr (222)	Al_2O_3, sputter
$Pb(Zr_{0.82}Ti_{0.18})O_3$	177.2	13.5, 25.2	11.43	Pv (110)	Al_2O_3, sputter
$Pb_{0.98}Nb_{0.04}(Zr_{0.2}Ti_{0.8})_{0.96}O_3$	177.2	11.4, 23.3	2.57	Pv (100)	Platinized Si, sol gel
$Pb_{0.91}La_{0.09}(Zr_{0.65}Ti_{0.35})_{0.98}O_3$	291.0	10.0, 12	1.07	Pv (100)	Platinized Si, sol gel
$Pb_{0.85}La_{0.15}Ti_{0.96}O_3$	308.2	0.0, 0.0	5.11	Pv(100)	Platinized Si, sol gel

crystals.[16] Note that annealed PZT56 shows a small amount of α-PbO phase, which formed during annealing, as shown in Fig. 1(b).[17]

B. Spectroscopic ellipsometry

We modeled the sample structures as surface roughness layer, main layer, and substrate. To model the surface roughness layer, we used an effective-medium approximation with a mixture of the main layer and voids. The effective dielectric function was calculated by the Bruggeman effective-medium approximation (EMA),[18]

$$f_{pzt}\frac{\epsilon_{pzt} - \epsilon^{eff}}{\epsilon_{pzt} + 2\epsilon^{eff}} + f_{void}\frac{\epsilon_{void} - \epsilon^{eff}}{\epsilon_{void} + \epsilon^{eff}} = 0, \quad (1)$$

where the effective dielectric function of the rms roughness layer was denoted by ϵ^{eff}, and dielectric functions (volume fractions) of PZT phase and voids are denoted, respectively, as ϵ_{pzt} (f_{pzt}) and ϵ_{void} (f_{void}). Details are shown in Table II.

The dielectric function of the main PZT layer was fitted using the POC model, in which the dielectric function is written as the summation of m energy-bounded, Gaussian-broadened polynomials and P poles accounting for the index effects due to absorption outside the model region.[19] The advantage of the POC model is that we can determine simultaneously both the band-gap parameters and the dielectric function from the pseudodielectric function. The POC model equation is Kramers-Kronig consistent, and is given by

$$\epsilon(\omega) = \epsilon_1(\omega) + i\epsilon_2(\omega) = 1$$

$$+ i\sum_{j=1}^{m}\int_{Emin}^{Emax} W_j(E)\Phi(\hbar\omega, E, \sigma_j)dE$$

$$+ \sum_{j=m+1}^{m+P+1}\frac{A_j}{(\hbar\omega)^2 - E_j^2}, \quad (2)$$

where

$$\Phi(\hbar\omega, E, \sigma) = \int_0^\infty e^{i(\hbar\omega - E + i2\sigma^2 s)s}ds - \int_0^\infty e^{i(\hbar\omega + E + i2\sigma^2 s)s}ds$$

$$= \sqrt{\frac{\pi}{8\sigma^2}}[e^{-y_1^2} + e^{-y_1^2}\text{erf}(iy_1)$$

$$- e^{-y_2^2} - e^{-y_2^2}\text{erf}(iy_2)], \quad (3a)$$

$$y_1 = \frac{\hbar\omega - E}{2\sqrt{2}\sigma}, \quad y_2 = \frac{\hbar\omega + E}{2\sqrt{2}\sigma}, \quad (3b)$$

$$W_j(E) = \sum_{k=0}^{N} P_{j,k}E^k u(E - a_j)u(b_j - E), \quad (4)$$

where $u(x)$ the unit step function. Here E_j, σ_j, and A_j are the energy threshold, broadening, and amplitude, respectively, for the jth band-gap structure.

The SCP model assumes simple parabolic dispersion relations for the valence and conduction bands and was developed by Cardona[20] and Aspnes.[21] This model provides accurate CP parameters such as energy threshold, broadening, amplitude, and excitonic phase angle. The SCP line-shape equation is given by[22]

$$\epsilon(\hbar\omega) = C - Ae^{i\Phi}(\hbar\omega - E + i\Gamma)^n, \quad (5)$$

where the CP is described by the amplitude A, threshold energy E, broadening Γ, and the excitonic phase angle Φ. The exponent n takes the values of $-1/2$ for one-dimensional (1D), 0 [logarithmic, i.e., $\ln(\hbar\omega - E + i\Gamma)$] for two-dimensional (2D), and $1/2$ for three-dimensional (3D) CP's. Discrete excitons are represented by $n = -1$. Here the excitonic phase angle Φ represents a coupling between the discrete exciton states and continuum band states. To remove the background contribution, we fit the second derivative of the dielectric function with respect to energy $[d^2\epsilon/d(\hbar\omega)^2]$ using the SCP model.

Figure 2 shows the pseudodielectric functions of (a) PZTs and (b) PLT and doped PZTs. The three band-gap peaks are identified as E_a, E_b, and E_c, respectively. The band-
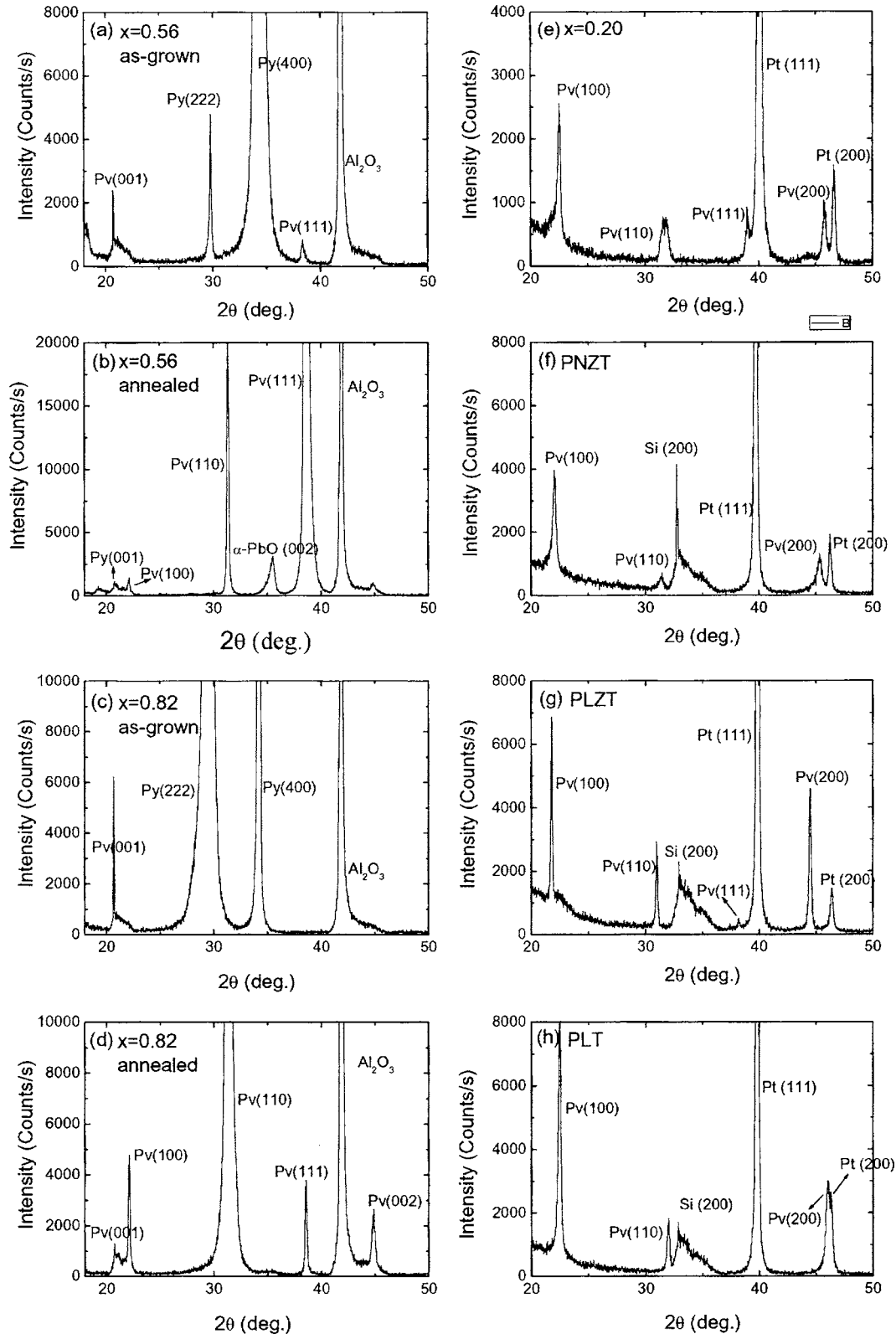
FIG. 1. X-ray data of the PZT, PLT, and doped PZT samples: PZT56 (a) as sputter grown and (b) annealed, and PZT82 (c) as sputter grown and (d) annealed. Others are grown by sol-gel method: (e) PZT20, (f) PNZT, (g) PLZT, and (h) PLT. Pv and Pr designate perovskite and pyrochlore phases, respectively.

gap peaks are more clearly discerned in the derivative spectra of the fitted PZT dielectric functions as shown in Figs. 5 and 6. Pseudodielectric functions in the spectral range below 4 eV were dominated by very strong interference patterns for sol-gel-grown PZT thin films on platinized silicon wafers, suggesting very abrupt interfaces. In the case of sputter-deposited PZTs on sapphire substrates, the interference patterns were not so strong suggesting relatively rougher interfaces.

Figure 3 is the measured ellipsometric parameter Ψ measured at 70° angle of incidence for the PZTs, PLT, and doped PZT samples and the best-fit curves using layer modeling as

TABLE II. Band-gap energies estimated by POC and SCP models. The error bars are ±0.02 eV within 95% reliabilities.

	E_a POC (SCP)	E_b POC (SCP)	E_c POC (SCP)
$Pb(Zr_{0.2}Ti_{0.8})O_3$	3.90 (3.87)	4.33 (4.38)	6.79 (6.79)
$Pb(Zr_{0.56}Ti_{0.44})O_3$, as grown	3.77 (3.75)	3.80	6.66
$Pb(Zr_{0.56}Ti_{0.44})O_3$	3.92 (3.91)	4.46 (4.63)	6.06 (6.07)
$Pb(Zr_{0.82}Ti_{0.18})O_3$, as grown	3.73 (3.85)	3.82	6.57
$Pb(Zr_{0.82}Ti_{0.18})O_3$	3.95 (3.90)	4.51 (4.67)	6.65 (6.71)
$Pb_{0.98}Nb_{0.04}(Zr_{0.2}Ti_{0.8})_{0.96}O_3$	3.98 (4.13)	4.29	6.79 (6.81)
$Pb_{0.91}La_{0.09}(Zr_{0.65}Ti_{0.35})_{0.98}O_3$	4.10 (4.08)	4.94	6.41 (6.74)
$Pb_{0.85}La_{0.15}Ti_{0.96}O_3$	4.20 (4.21)	4.84	6.54 (6.66)

FIG. 3. Ψ (solid lines) measured at 70° angle of incidence and their curve fits (dotted lines) using layer modeling for $Pb(Zr_xTi_{1-x})O_3$ (x=0.20, 0.56, 0.82), PNZT, PLZT, and PLT.

described above. The fitting was performed using the POC model. Note that we assumed isotropic dielectric function for PZTs, even though x-ray-diffraction data suggested various main crystal orientations for different PZTs. The ellipsometric parameters Ψ and Δ can be converted to the pseudodielectric functions using a simple formula.[23] The raw data and curve fits matched very well and they could not be discerned separately in Fig. 3. The fit parameters are shown in Tables I and II. The lowest energy peak of all the PZTs, PLT, and doped PZTs could be fitted as double peaks rather than a single peak using the POC model. Note that Yang et al.[7] fitted the peak as a single peak. The fitted band-gap values of the POC model are shown in Table II.

The fitting parameters were the thickness of the thin film and the volume fraction of each constituent as well as the dielectric functions of PZTs. The parameter values were de-
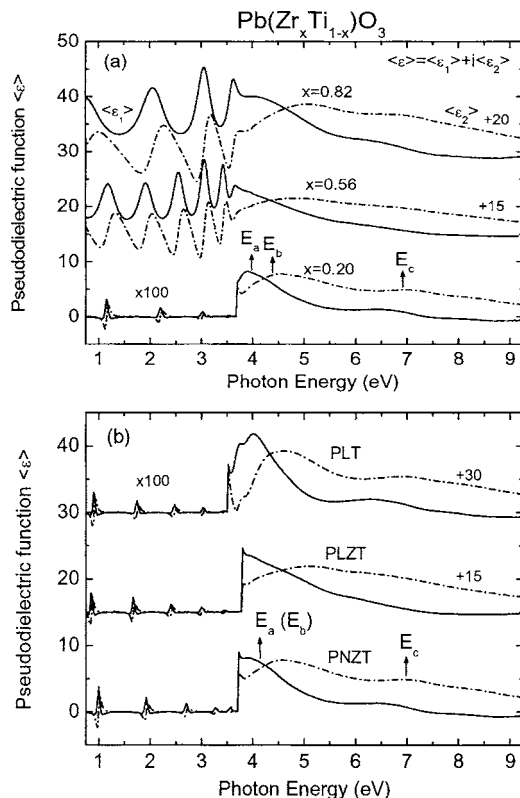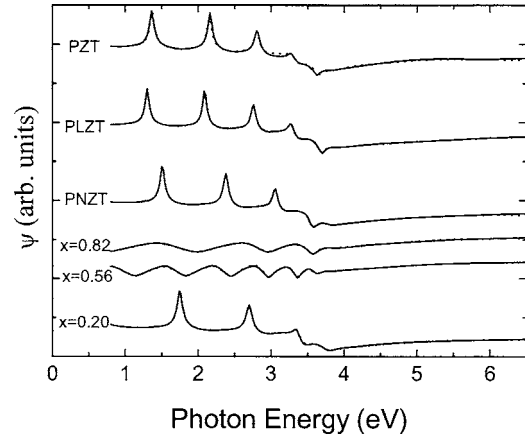

FIG. 2. Pseudodielectric functions in the spectral range of 0.8–9.25 eV: (a) $Pb(Zr_xTi_{1-x})O_3$, x=0.20, 0.56, 0.82, and (b) PNZT, PLZT, and PLT. The three band-gap peaks are identified as E_a, E_b, and E_c, respectively.

termined using the nonlinear Levenberg-Marquardt algorithm, which minimized χ^2, a measure of the goodness of the fit,

$$\chi^2 = \frac{1}{2N-m-1}\sum_{i=1}^{N}|\langle\epsilon\rangle_i^{exp}-\langle\epsilon\rangle_i^{mod}|^2, \quad (6)$$

where N is the number of data points, m is the number of the fitting parameters, and $\langle\epsilon\rangle^{exp}$ and $\langle\epsilon\rangle^{mod}$ are the measured and modeled pseudodielectric functions, respectively. The modeled pseudodielectric function $\langle\epsilon\rangle^{mod}$ is a function of the thickness of the thin film, the volume fraction, and the dielectric functions of the void and PZT materials. The ellipsometrically fitted parameters are listed in Tables I and II.

The layer fitting was excellent when we fit the pseudodielectric functions in the spectral range between 0.8 and 6.5 eV. However, when we attempted the fitting in the entire spectral range of 0.8–9.25 eV, it was not very successful for some PZT or doped PZT thin films. The fitting in the DUV spectral range was not satisfactory possibly because the interference pattern in the NIR-visible (VIS) range was dominant. Therefore, we fitted the UV-DUV region separately in the 4.0–9.25 eV range using the POC model. We assumed a surface roughness layer with a mixture of 50% void and 50% main layer for the layer modeling in the UV-DUV spectral range. The fitting was so successful that the raw data and fit curve could not be discerned from each other. We note that the fitting in the UV-DUV spectral range is sensitive to the surface roughness layer, but insensitive to the thickness of the main layer because of very small penetration depth of the light. The band-gap energy E_c is listed inTable II.

In Table I, the thicknesses of surface roughness determined by ellipsometry is much larger than the rms roughness values determined by AFM. However, the increase of roughness of PZTs grown on the Al_2O_3 substrates compared with those grown on platinized silicon is qualitatively consistent for both ellipsometry and AFM.

Figure 4 is the fitted dielectric function of each PZT layer. The dielectric function of the PLT layer had the narrowest peak among all the PZTs and doped PZT layers. Hence, if we assume that the broadening comes from com-
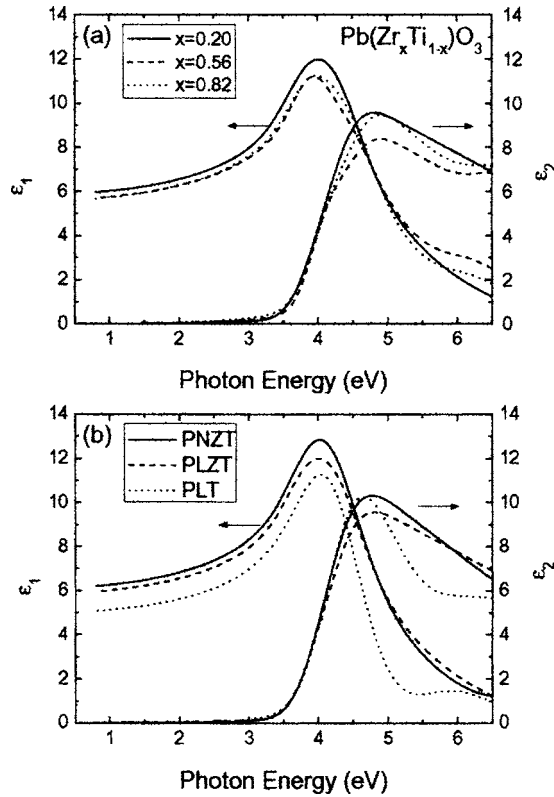
FIG. 4. Fitted dielectric function of the PZT layers in the spectral range of 0.8–6.5 eV: (a) PZTs and (b) PNZT, PLZT, and PLT.

FIG. 5. Plot of the second derivative of dielectric functions and their fits in the NIR-VIS-UV spectral range. The fitted band-gap energies E_a and E_b are marked with arrows.

positional disorder, the chemical difference between Pb^{82} ($6s^2 6p^2$) and La^{57} ($5d^1 6s^2$) should be smaller than that between Zr^{40} ($4d^2 5s^2$) and Ti^{22} ($3d^2 4s^2$). However, Pb and La have different valences of Pb^{2+} and La^{3+}, and will cause vacancies of Pb and La to meet the criteria of neutrality.[24] Note that Zr^{4+} and Ti^{4+} have the same valences. Therefore, the narrow peak of PLT is surprising because the compositional disorder should be larger for PLT. The dielectric functions of PLZT and PNZT are similar to those of PZTs even with additional elements of La^{3+} or Nb^{5+} atoms. Note that Pb and La occupies the A site, and that Nb, Zr, and Ti occupies the B site.

Figure 5 is the plot of second derivative of dielectric functions and their fit using SCP model. Figure 6 is the same as Fig. 5 for the DUV spectral range on PZT20, PLT, and doped PZTs which were grown on platinized silicon using sol-gel methods. The fitted band-gap energies (E_a and E_b in Fig. 5 and E_c in Fig. 6) are marked with arrows. Yang *et al.*[7] assumed that the lowest optical structure near 4 eV is a single peak in their layer modeling of the dielectric function of PZTs. However, our POC model fitting shows that the 4 eV structure of the PZTs have double peaks as verified in the second derivative spectra of the fitted dielectric function shown in Fig. 5(a). In Fig. 5(a), PZT56 and PZT82 have distinctively double peak structures probably because sputter-grown PZTs have higher crystallinity than those grown by the sol-gel method as shown in Fig. 1.

In order to estimate the band-gap parameters accurately, we took the second derivative of the dielectric functions and fitted using the SCP model. We found that an exciton fit was
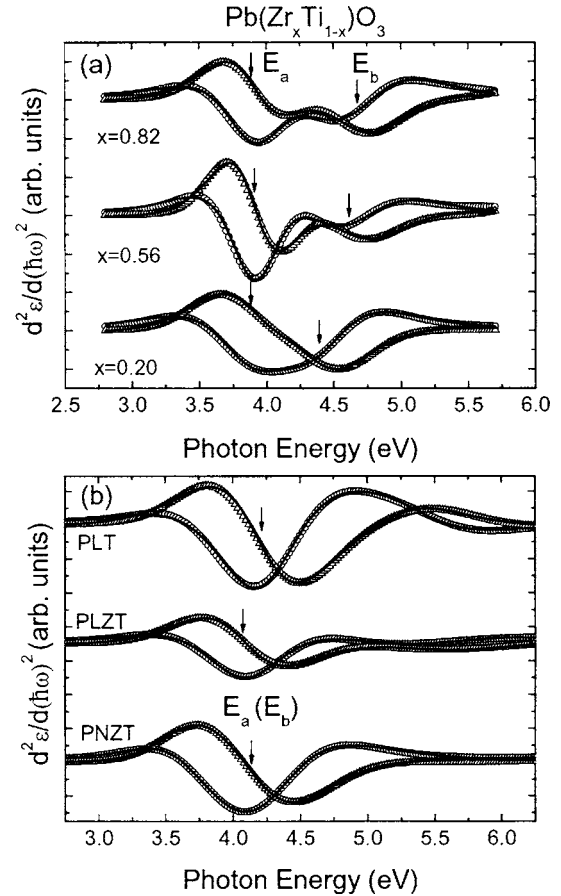
the best fit for E_a, E_b, and E_c rather than a one-, two-, or three-dimensional CP fit. The CP (band gap) energies were denoted as E_a, E_b, and E_c for both the perovskite and pyrochlore phases in the order of increasing energy for simplicity. Excitonic interaction appears strong in the perovskite oxide similar to the semiconductor oxide ZnO. Strong ionic bonding rather than covalent bonding may be responsible for the strong excitonic interaction. Actually, perovskite oxide can be classified as a semiconductor because the band gap is near 4 eV which is slightly larger than that of ZnO ($\sim$3.35 eV at
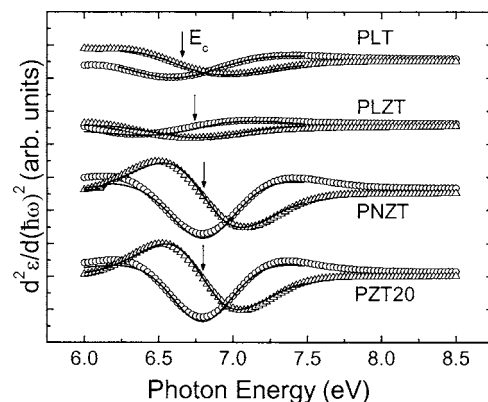

FIG. 6. Plot of the second derivative of dielectric functions and their fits in the DUV spectral range for PZT20, PNZT, PLZT, and PLT grown on platinized silicon. The fitted band-gap energy E_c is marked with an arrow.
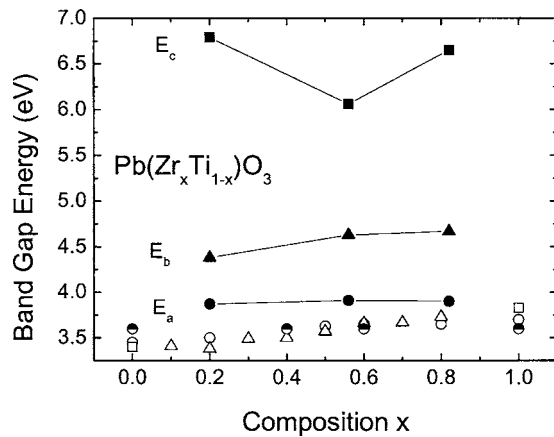
FIG. 7. Plot of band-gap energies for PZTs, PLT, and doped PZTs fitted (our own) and from literature. Filled symbols are from our data of spectroscopic ellipsometry (SE), and other symbols are unfilled circle [Peng *et al.* (Ref. 6)], unfilled triangle [Yang *et al.* (Ref. 7)], unfilled rectangle [Zametin (Ref. 25)], and half-filled circle [Moret *et al.* (Ref. 8)].

RT). Here the exciton may be Frenkel rather than Wannier type due to its strongly localized character.[22] The CP energies, listed in Table II, were determined using both the POC model and SCP model.

In Fig. 5(a), the apparent single peak in the $d^2\epsilon/d(\hbar\omega)^2$ spectra of PZT20 could be fitted much better assuming double peaks rather than a single peak in the POC model. For the doped PZTs and PLT, double-peak fitting in the SCP model provided two correlated, closely spaced band-gap energies. This may be due to the close overlap of the two broad peaks. Therefore, we fitted the optical structures of PNZT, PLZT, and PLT using a single peak rather than a double peak. The fitted band-gap values are listed in Table II. We also performed SCP fitting to the second derivative of the dielectric function in the DUV spectral range and could fit the higher band-gap energy E_c.

IV. DISCUSSION

Figure 7 plots the CP energies E_a, E_b, and E_c as a function of Zr composition for PZTs. We also plotted the band-gap energy values from literature. With increasing Zr composition, the band gap increased slightly for E_a and E_b. This result is consistent with literature, where the band-gap energies either increased slightly or did not change.[6–8,25] Our fitted band-gap values are in general larger than the literature values. The slight increase or near constancy of the band-gap energies, E_a and E_b, of PZTs as a function of the Zr content suggests that the substitution of Ti by Zr does not change appreciably the electronic band structure of PZT materials. The band-gap energy (E_c) does not show any sign of monotonic behavior.

The reason why the band-gap energy values of this work are higher than those available in literature may be attributed to the fact that the band-gap energies were determined accurately using SCP fitting rather than the band edge [α^2 (Ref. 6)] or optical band-gap [$(\alpha E)^2$ (Ref. 7)] values determined from optical absorption spectra. We checked this by plotting the absorption coefficient from our optical constant values.

From the estimated refractive index values ($\sqrt{\epsilon}=n+ik$), we calculated the absorption coefficient (α). Using the absorption coefficient so determined, we determined the direct band gap (E_g) using the relation $\alpha^2 \propto (E-E_g)$ (Ref. 6) and also determined the optical band gap (E_{opt} using the relation $(\alpha E)^2 \propto (E-E_{opt})$.[7] The fitted band-edge energy values were smaller by about 0.2 and 0.1 eV, respectively, than E_a, i.e., the ellipsometrically determined CP energy values. Our band-gap energy is about 0.1–0.4 eV larger than the literature values. Peng *et al.*[6] and Yang *et al.*[7] estimated the band-edge energies using the absorption spectra, which were measured directly or derived from the modeled ellipsometric data. Therefore their values are smaller than our CP energies.

The ellipsometry data of Yang *et al.* cover only up to 5 eV. Moreover, their fitting using the Forouhi-Bloomer model gave only a single peak in contrast to our double peak fitting. The x-ray data of annealed PZTs of Yang *et al.*[7] show a significant amount of remaining pyrochlore phase as well as a perovskite phase. This may explain why they could fit the optical structure as a single peak rather than as double peak. Our annealed PZTs show only the perovskite phases. In Table II, sputter-grown PZT56 and PZT82 thin films without annealing have essentially single peaks near 4 eV probably because the pyrochlore phase is dominant in the films as shown in x-ray data of Figs. 1(a) and 1(c).[26] In Table II and Fig. 5, small amounts of Nb and La dopants do not cause an appreciable shift of band-gap energies for E_a, E_b, and E_c.

The band-gap energies of ferroelectric thin films can be affected by the strain and electric field. In ferroelectric thin films, the strain and electric field are correlated due to inherent piezoelectricity. Strains can arise from both the lattice mismatch and difference in thermal expansion coefficient between the films and substrate. In analyzing the Zr composition dependence of the band-gap energies of PZT in Fig. 7 and Table II, we did not include the strain and electric effect. In Table II, the band-gap energies of E_a of PNZT and PLZT did not change within error bars compared to those of PZT20 and PZT56, respectively. This result is not surprising considering the low concentration of Nb (4%) and La (9%). This result shows that the substitution of Ti (Zr) by Nb or the substitution of Pb by La does not affect much the band-gap energy of the corresponding PZT.

Band-structure calculations

To understand the Zr composition dependence of the PZT band-gap energies in Fig. 7, we have carried out first-principles band-structure calculations for bulk PZT, neglecting the effect of strain and electric field. Even though the band structures of the thin films will be affected by strain and electric-field effects, the band calculations will give qualitative information on the Zr composition dependence of PZT band-gap energies.

The calculations are performed within local-density approximation (LDA) as implemented in the Vienna *ab initio* Simulation Package (VASP) code.[26–28] The cutoff energy for the basis functions is 396 eV. The calculated lattice constants for the two end-point materials $PbTiO_3$ (PTO) and $PbZrO_3$ (PZO) are 3.87 and 4.11 Å, respectively, in good agreement
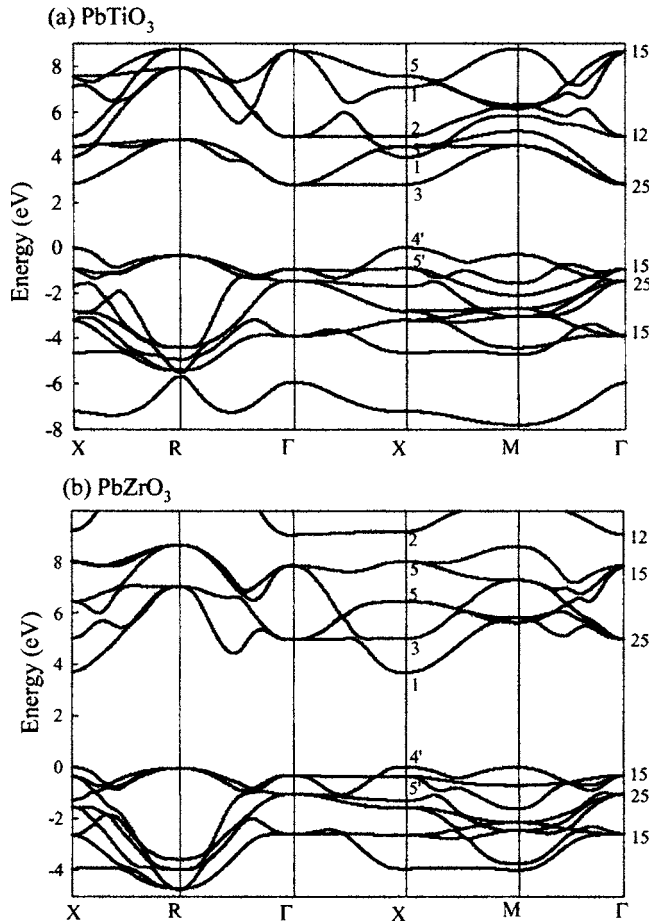
FIG. 8. Calculated band structure of (a) PbTiO$_3$ and (b) PbZrO$_3$. The energy zero is at the top of the valence band.
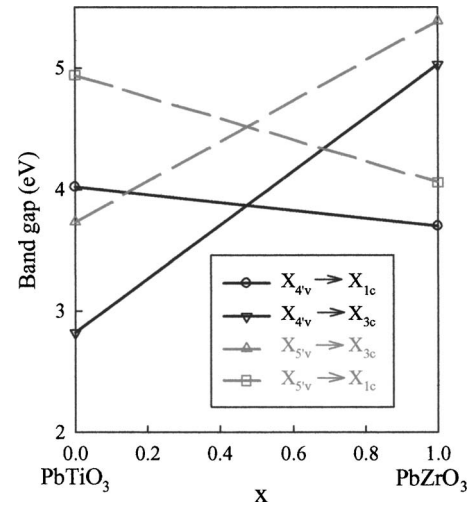

FIG. 9. Calculated band-gap energies of PZT as a function of Zr composition. The lines assume linear interpolation between the two end-point compounds, PbTiO$_3$ and PbZrO$_3$.

with the experimental values of 3.96 and 4.13 Å. The LDA calculated band gaps are smaller than the experimental band gaps due to the well-known LDA band-gap error. To facilitate direct comparison with experiment, we have shifted uniformly all the conduction band energy by 1.37 eV. Figures 8(a) and 8(b) are the calculated band structures for PTO and PZO at experimental lattice constants. The calculated results show that both PTO and PZO have direct band gaps at the X point. The valence-band maximum[28,29] (VBM) at X has the $X_{4'v}$ symmetry and is mostly a mixture of O p and Pb s states. However, for PTO the conduction-band minimum (CBM) at X is an X_{3c} state,[28,29] whereas in PZO the CBM is an X_{1c} state. X_{3c} is a transition metal (TM), Ti and Zr, d state. Therefore, its energy is sensitive to the TM concentrations. Because the Zr $4d$ atomic energy level is about 0.73 eV higher than the Ti $3d$ level, when the Zr concentration increases, the X_{3c} level also increases as shown in Fig. 9. Figure 9 plots the calculated band-gap energies of PZT as a function of Zr composition. The X_{1c} state is mostly an O s and Pb p state, and the VBM has the Pb s and O p character, thus their energy levels are not sensitive to the TM substitution. We find that relative to VBM the X_{1c} gap energy decreases slightly when Zr concentration increases (Fig. 9). It is interesting to note that the energy of the bottom of the conduction-band state at Γ ($\Gamma_{25'c}$) is nearly identical to the X_{3c} state because they have the same atomic character (TM

d). Similarly, the top of the valence-band state at Γ (Γ_{15v}) and the $X_{5'v}$ state are nearly pure O p states, so they also have almost the same energy.

Due to the symmetry, the dipole transition-matrix element squared $|\langle VBM|P|X_{3c}\rangle|^2$ is nearly zero (Table III), but is large for $|\langle VBM|P|X_{1c}\rangle|^2$. This indicates that for PTO- or Ti-rich PZT the measured optical band gap (determined mostly by transition to the vicinity of X_{1c} state) is larger than the fundamental band gap (determined by the X_{3c} state). By comparing with experimental data, we suggest that the E_a band gap determined by the ellipsometrical measurement can be attributed mostly to the $X_{4'v} \rightarrow X_{1c}$ transitions. The calculated $X_{4'v} \rightarrow X_{1c}$ band-gap energy decreases slightly when Zr concentration increases. However, because the magnitude of the transition-matrix elements increases when the k points move away from the X point for the fundamental band gap along the X-Γ and X-M directions, the actual optical band gap for PTO is smaller than the $X_{4'v} \rightarrow X_{1c}$ energy difference. This can be seen clearly from the calculated absorption coefficient (Fig. 10), where, we see that the threshold energy of E_a or PTO and PZO is nearly constant at about 3.85 eV, in agreement with experimental data in Fig. 7.

Robertson *et al.*[29,30] calculated the band structure of PZTs and showed a small increase of $X_{4'v} \rightarrow X_{1c}$ band-gap energy with increasing Zr composition. They attributed the increase of the band-gap energy to the increase of the X_{1c} conduction-band energy due to an increase of the lattice constant as Zr concentration increases. Although our results are similar to theirs in that the optical band gaps are almost

TABLE III. Calculated optical transition-matrix element squared for several band-edge transitions in PTO and PZO.

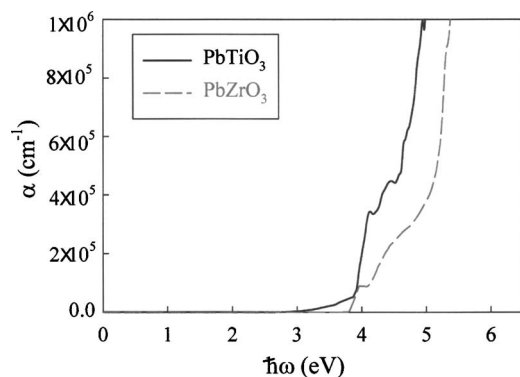|	PbTiO$_3$	PbZrO$_3$
$\|\langle X_{4'v}\|P\|X_{3c}\rangle\|^2$(eV)	0.0	0.0
$\|\langle X_{4'v}\|P\|X_{1c}\rangle\|^2$(eV)	0.235	0.180
$\|\langle X_{5'v}\|P\|X_{3c}\rangle\|^2$(eV)	0.033	0.032
$\|\langle X_{5'v}\|P\|X_{1c}\rangle\|^2$(eV)	0.131	0.144

FIG. 10. Calculated absorption spectra for PbTiO$_3$ and PbZrO$_3$.

constant, independent of the Zr compositions, we find the opposite trend for the $X_{4'v} \rightarrow X_{1c}$ transition energy, i.e., it decreases with the Zr concentration. However, our results are similar to those calculated by King-Smith and Vanderbilt,[30,31] which are consistent with our finding that the $X_{4'v} \rightarrow X_{1c}$ transition energy actually decreases as the lattice, constant increases. We find that although the $X_{4'v} \rightarrow X_{3c}$ transition is nearly forbidden, the transitions from the second valence band ($X_{5'v}$) to both conduction states X_{1c} and X_{3c} are allowed. Figure 9 plots the variations of $X_{5'v} \rightarrow X_{1c}$ and $X_{5'v} \rightarrow X_{3c}$ as a function of Zr concentration. As discussed earlier, the $\Gamma_{15v} \rightarrow \Gamma_{25'c}$ transition (not shown) is nearly identical to that of $X_{5'v} \rightarrow X_{3c}$ transition because they have similar wave-function characters. We find that $X_{5'v} \rightarrow X_{1c}$ transition energy decreases as Zr concentration increases, whereas the $X_{5'v} \rightarrow X_{3c}$ transition energy increases as the Zr concentration increases. We suggest that the measured E_b band gap can be due to transitions along the X-Γ and X-M lines originating from these two transitions. From the calculated absorption spectra in Fig. 10, we see that the E_b band-gap energy increases from PTO to PZO, also consistent with experimental observation.

We caution that more detailed band-structure calculations and experimental estimate of the strain and electric field in the thin films are required for quantitative comparison between the calculated and the experimentally measured band-gap energies. For example, for band-structure calculations we did not include the effect of strain and electric field, and assumed cubic crystalline phase although PZT crystals have tetragonal (Zr$<$52%) and rhombohedral phases (Zr $>$52%).

V. CONCLUSION

We measured the pseudodielectric functions in the visible-deep ultraviolet spectral range of Pb(Zr$_x$Ti$_{1-x}$)O$_3$ ($x=0.2, 0.56, 0.82$), Pb$_{0.98}$Nb$_{0.04}$(Zr$_{0.2}$Ti$_{0.8}$)$_{0.96}$O$_3$, Pb$_{0.91}$La$_{0.09}$(Zr$_{0.65}$Ti$_{0.35}$)$_{0.98}$O$_3$, and Pb$_{0.85}$La$_{0.15}$Ti$_{0.96}$O$_3$ thin films grown on platinized silicon substrates using a sol-gel method and grown on (0001) sapphire using a rf sputtering method. Using the POC model method, we estimated the dielectric functions of the ferroelectric thin films. Taking the second derivative of the fitted layer dielectric functions and using the standard critical-point model, we determined the parameters of the critical points. The lowest energy peak

near 4 eV is fitted as a double peak for annealed PZTs due to perovskite phase. Sputter-grown PZTs without annealing had mainly a pyrochlore phase and the lowest band-gap peak was fitted as a single peak. We also examined the effect of dopants Nb and La, which substitute at Pb sites. We discussed the change of the CP parameters for PZTs in comparison to band-structure calculations. The near constancy of the band-gap energy (E_a) is verified by both ellipsometric spectra and LDA band structure calculations.

[1]K. Uchino, *Ferroelectric Devices* (Marcel Dekker, New York, 2000).
[2]Y. Xu, *Ferroelectric Materials and Their Applications* (North-Holland, Tokyo, 1991).
[3]B. Li, P. T. Lai, G. Q. Li, S. H. Zheng, and M. Q. Hwang, Smart Mater. Struct. **9**, 498 (2000).
[4]I. K. Yoo, in *Ferroelectric Thin Films*, edited by S. Hong (Kluwer Academic, New York, 2004) p. 3.
[5]R. Ramesh, S. Aggarwal, and O. Auciello, Mater. Sci. Eng., R. **32**, 191 (2001), and references therein.
[6]C. H. Peng, J.-F. Chang, and S. B. Desu, Mater. Res. Soc. Symp. Proc. **243**, 21 (1992).
[7]S. Yang, D. Mo, and X. Tang, Ferroelectrics **287**, 35 (2003).
[8]M. P. Moret, M. A. C. Devillers, K. Wörhoff, and P. K. Larsen, J. Appl. Phys. **92**, 468 (2002).
[9]L. Pintile, I. Boerasu, M. J. M. Gomes, and M. Pereira, Thin Solid Films **458**, 114 (2004).
[10]I. Boerasu, L. Pintile, M. Pereira, M. I. Vasilevskiy, and M. J. M. Gomes, J. Appl. Phys. **93**, 4776 (2003).
[11]S. B. Krupanidhi, H. Hu, and V. Kumar, J. Appl. Phys. **71**, 376 (1992).
[12]S. Dutta, R. N. P. Choudhary, P. K. Sinha, and A. K. Thakur, J. Appl. Phys. **96**, 1607 (2004), and references therein.
[13]K. W. Kwok, R. C. W. Tsang, H. L. W. Chan, and C. L. Choy, J. Appl. Phys. **95**, 1372 (2004).
[14]S. Bhaskar, S. B. Majumder, and R. S. Katiyar, Appl. Phys. Lett. **80**, 3997 (2002).
[15]C. Millon, C. Malhaire, and D. Barbier, Sens. Actuators, A **113**, 376 (2004).
[16]B. Jaffe, W. R. Cook, and H. Jaffe, *Piezoelectric Ceramics* (Academic, London, 1971).
[17]B. Thangaraju and P. Kaliannan, Semicond. Sci. Technol. **15**, 542 (2000).
[18]D. E. Aspnes, Thin Solid Films **89**, 249 (1982).
[19]B. Johs, C. M. Herzinger, J. H. Dinan, A. Cornfeld, and J. D. Benson, Thin Solid Films **313/314**, 137 (1998).
[20]M. Cardona, in *Modulation Spectroscopy, Solid State Physics*, edited by F. Seitz, D. Turnbull, and H. Ehrenreich (Academic, New York, 1969), p. 65.
[21]D. E. Aspnes, *Handbook on Semiconductors* (North Holland, Amsterdam, 1980), Vol. 2, p. 109.
[22]P. Lautenschlager, M. Garriga, L. Viña, and M. Cardona, Phys. Rev. B **36**, 4821 (1987), and reference therein.
[23]R. M. A. Azzam and N. M. Bashara, *Ellipsometry and Polarized Light* (Elsevier Science, New York, 1987).
[24]G. H. Haertling, J. Am. Ceram. Soc. **82**, 797 (1999).

[25]V. I. Zametin, Phys. Status Solidi B **124**, 625 (1984).

[26]H. Lee, Y. S. Kang, S.-J. Cho, B. Xiao, H. Morkoç, and T. D. Kang, Appl. Phys. Lett. **86**, 262902 (2005)..

[27]G. Kresse and J. Hafner, Phys. Rev. B **47**, 558 (1993).

[28]G. Kresse and J. Furthmüller, Phys. Rev. B **54**, 11169 (1996).

[29]For PTO, the bottom of the conduction band at Γ is actually 2 meV lower than the X_{3c} state and in PZO the top of valence band at M is actually 12 meV higher than the $X_{4'v}$ state. For practical reasons, we will consider PTO and PZO as direct gap material with VBM and CBM at X point.

[30]J. Robertson, W. L. Warren, and B. A. Tuttle, J. Appl. Phys. **77**, 3975 (1995).

[31]R. D. King-Smith and D. Vanderbilt, Phys. Rev. B **49**, 5828 (1994).